Heliyon 10 (2024) e31969

Contents lists available at ScienceDirect

Heliyon

journal homepage: www.cell.com/heliyon

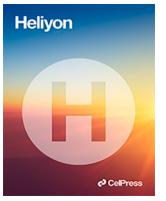

Research article

CircRNA hsa_circ_0069,399 as a potential clinical prognostic marker in laryngeal squamous cell carcinoma

Zhipeng Mi [a], Wulin Wen [b], Fan Guo [a], Qiangyou Shi [c], Chao Long [d], Yu Zhou [b], Ruixia Ma [b,*]

[a] The Second Clinical Medical College, Ningxia Medical University, 750000 Yinchuan, Ningxia, China
[b] Yinchuan First People's Hospital, Otolaryngology Head and Neck Surgery Hospital, 750000 Yinchuan, Ningxia, China
[c] Department of Otolaryngology Head and Neck Surgery, Gansu Maternal and Child Health Care Hospital, 730050 Lanzhou, Gansu, China
[d] Yueyang City Central Hospital Otolaryngology Head and Neck Surgery, 414000 Yueyang, Hunan, China

ARTICLE INFO

Keywords:
Laryngeal squamous cell carcinoma
circRNA
hsa_circ_0069399
ceRNA

ABSTRACT

Objective: Circular RNAs (circRNAs) significantly influence the invasion, metastasis, gene expression, proliferation, and apoptosis of tumor cells. However, the roles of circRNAs in laryngeal squamous cell carcinoma (LSCC) remain largely unexplored. This study aims to examine circRNA expression patterns in LSCC and adjacent non-tumorous tissues, with the goal of uncovering potential biomarkers for LSCC.

Methods: Tissue samples were collected from both the tumor and adjacent normal tissues of ten patients who had undergone surgical resection. The profiling of circRNAs was conducted through transcriptomic sequencing and analytical bioinformatics approaches. A ternary regulatory network based on the competitive endogenous RNA (ceRNA) hypothesis was established, linking target circRNAs to clinical immunohistochemical parameters for comparison. Verification of target circRNAs in LSCC tissues was performed using quantitative real-time PCR (RT-qPCR), whereas target mRNAs were analyzed through immunohistochemistry.

Results: A total of 126 significantly different circRNAs were identified, including 40 up-regulated genes and 86 down-regulated genes. Furthermore, 92 circRNA-miRNA-mRNA regulatory relationship axes related to clinical immunohistochemical indicators were found based on 5 candidate circRNAs. Interestingly, all axes related to the target genes MKI67 and TP53 were found to compete with the same circRNA: hsa_circ_0069,399. Further verification confirmed that the hsa_circ_0069,399 expression was overtly upregulated in tumor tissues from LSCC patients, which was consistent with the sequencing results.

Conclusion: hsa_circ_0069,399 could be a potential prognostic marker for LSCC.

1. Introduction

Laryngeal cancer (LC) is a significant form of head and neck malignancy, contributing substantially to cancer-related morbidity and mortality worldwide. Annually, it is estimated that LC affects approximately 276,000 individuals, posing significant health challenges across diverse populations [1]. The clinical management of LC, depending on the stage at diagnosis, varies from organ-preserving

* Corresponding author.
E-mail addresses: mm296390383@163.com (Z. Mi), maruixia4368@sina.com (R. Ma).

https://doi.org/10.1016/j.heliyon.2024.e31969
Received 26 February 2024; Received in revised form 21 May 2024; Accepted 24 May 2024
Available online 25 May 2024

surgeries to more radical treatments like total laryngectomy, which profoundly impacts patients' quality of life [2–4]. Given the asymptomatic nature of early-stage LC and the potential for improved outcomes with earlier diagnosis, there is a compelling need for identifying reliable biomarkers. These biomarkers hold the promise not only for early detection but also for providing insights into the disease's prognosis and guiding personalized therapeutic strategies.

In recent years, circular RNAs (circRNAs), a novel class of endogenous non-coding RNA that are highly stable and conserved across species, have emerged as potential biomarkers for various diseases, including cancer. Unlike linear RNAs, circRNAs form a covalently closed continuous loop, which confers resistance to exonuclease-mediated degradation, making them ideal candidates for biomarker discovery. They are involved in modulating gene expression at the post-transcriptional level, serving functions ranging from acting as microRNA sponges to interacting with RNA-binding proteins [5]. The implication of circRNAs in pivotal biological processes, such as cell proliferation, migration, and invasion, underscores their relevance in cancer biology [6,7]. Despite the increasing evidence supporting circRNAs' role in cancer, their utility as biomarkers in laryngeal cancer has not been widely studied, indicating a significant gap in the current research landscape.

This manuscript seeks to address this gap by investigating the expression patterns of circular RNAs in laryngeal squamous cell carcinoma (LSCC) tissues compared to adjacent normal tissues. Specifically, it focuses on identifying potential circRNA biomarkers that could contribute to the understanding, diagnosis, and prognosis of LSCC. By leveraging high-throughput RNA sequencing and bioinformatics analyses, this study aims to elucidate the regulatory networks involving circRNAs and their associations with clinical outcomes in LSCC patients. In doing so, it hopes to pave the way for innovative approaches to the diagnosis and treatment of laryngeal cancer, ultimately contributing to improved patient care and outcomes.

2. Materials and methods

2.1. Tumor tissue specimen

Tumor foci and adjacent non-tumorous tissues (>2 cm away from the tumor margin) were collected from ten patients diagnosed with laryngeal squamous cell carcinoma (LSCC) between January 2022 and December 2022 at the Otorhinolaryngology Head and Neck Surgery Department of Ningxia Medical University Affiliated Hospital. Immediately following its removal from the body, the specimen should be cleansed of any surface blood stains using normal saline, then immersed in a cryopreservation tube containing RNA fixative solution (RNAlater) (76,106, Qiagen, Germantown, MD, USA). It should then be stored in a refrigerator set to 4 °C overnight within an ice box to ensure thorough saturation of the tissue sample with the RNA fixation solution, before being transferred for long-term storage in a -80 °C freezer. Each tissue sample acquired from patients was accompanied by a definitive pathological diagnosis.

The criteria for case inclusion and exclusion were as follows: (1) The patient had not received radiotherapy or chemotherapy prior to surgery; (2) The postoperative pathological assessment confirmed the diagnosis of primary laryngeal squamous cell carcinoma, with the tumor localized to a single area; (3) Complete clinical data for the patient was available; (4) The RNA content of the tissue sample met the required standards upon analysis. The collection procedures were carried out with the informed consent of all patients under a protocol approved by the Medical Ethics Committee of Ningxia Medical University Affiliated Hospital (Approval No. 2022-147).

2.2. Extraction and purification of total RNA

LSCC tissues and normal mucosal tissues, preserved at -80 °C, were pulverized into powder in liquid nitrogen. Subsequently, total RNA was extracted from these tissues using the protocol specified by the Trizol reagent (15,596,018, Invitrogen, Waltham, MA, USA). Once dissolved in diethyl pyrocarbonate (DEPC)-treated distilled water, the RNA was further purified using an RNA purification kit (ER701-01, TransGen, Beijing, China). The purity and concentration of the RNA were assessed with the NanoDrop2000 spectrophotometer (NanoDrop2000, Thermo Fisher Scientific, Waltham, MA, USA), showcasing an OD260/280 ratio between 1.8 and 2.1, indicative of high-quality RNA. The integrity of the RNA samples were evaluated through 1 % formaldehyde denaturing gel electrophoresis before use.

2.3. RNA library construction and sequencing

Upon meticulously labeling and documenting pertinent details, ten pairs of LSCC tissues alongside their adjacent non-cancerous tissues were securely transported to the laboratory ensconced in dry ice, primed for high-throughput RNA sequencing. The handling and preservation of these samples were in strict adherence to the manufacturer's guidelines on RNA sample preparation and transportation (Cat # RS-122-2001, Illumina Inc, San Diego, USA). In alignment with the prescribed protocol, RNA extraction was carried out, followed by its conversion, amplification, and subsequent sequencing in a paired-end manner using the advanced Illumina Hiseq 4000 system (LC Bio, Hangzhou, China). This investigation harnessed the power of the Illumina sequencing technology platform to facilitate these processes.

2.4. Analysis of bioinformatics methods

In the initial phase of our analysis, we employed Cutadapt (GitHub, San Francisco, CA, USA) to eliminate reads contaminated by adapters, reads with low-quality bases, and reads with undetected bases. Subsequently, FastQC (Illumina, San Diego, CA, USA) was

utilized to verify the quality of the sequences. These refined reads were then aligned with the species' genome using both bowtie2 (v2.2.8, Johns Hopkins University, Baltimore, MD, USA) and Hisat2 (v2.0.4, Johns Hopkins University, Baltimore, MD, USA) for precise mapping, while tophat-fusion was applied to map the remaining unmapped reads to the genome. For the reconstruction of circRNAs from the mapped reads, we utilized CIRCExplorer2 (v2.2.6, Key Laboratory of Computational Biology, Shanghai, China) and CIRI (v1.0, Cloud-Seq, Inc., Shanghai, China), alongside tophat-fusion for identifying back-splicing reads among the unmapped sequences. This comprehensive approach enabled the identification of unique circRNAs across all samples. In the subsequent analytical stage, we leveraged the R software (version 3.3.3, R Foundation for Statistical Computing, Vienna, Austria) to filter out circRNAs exhibiting significant differential expression, characterized by an absolute log2 fold change (|log2FoldChange|) of at least 1 and a p-value of less than 0.05. This filtration process was crucial for constructing an expression profile and undertaking a feature analysis of the circRNAs. To visualize and interpret the overarching expression trends of circular RNAs, we conducted a volcano map analysis. A cluster map analysis was also performed to explore the expression similarities among different samples. Further, to elucidate the functional implications of these differentially expressed circRNAs, we carried out GO and KEGG enrichment analyses. These analyses were instrumental in providing functional annotations concerning biological functions, pathways, and diseases, thereby enriching our understanding of the roles played by these circRNAs.

2.5. Target gene prediction and construction of regulatory network

Based on the outcomes of our bioinformatics analysis, we identified circRNA molecules exhibiting significant differential expression. From this pool, we meticulously selected five circRNA molecules demonstrating the most pronounced differential changes and consistent expression across various groups as our candidate genes. This selection includes two circRNAs that were up-regulated and three that were down-regulated.

Initially, we identified differentially expressed circRNAs, miRNAs, and mRNAs through whole-transcriptome sequencing data analysis. Utilizing TargetScan and miRanda website, we then predicted the target genes for the five selected candidate circRNAs, focusing on miRNAs. By intersecting the predictions from both software tools, we established target relational pairs between circRNA and miRNA, as well as miRNA and mRNA. This approach facilitated the construction of several ternary network interaction axes for circRNA-miRNA-mRNA, based on miRNAs common to both sets. It was discovered that the five candidate circRNAs were involved in a total of 25,590 control relationships. Further analysis overlaid the clinical immunohistochemical pathological findings from 73 LSCC patients with the mRNAs implicated in these 25,590 regulatory relationships, revealing 92 circRNA-miRNA-mRNA axes associated with clinical immunohistochemical outcomes. To visually dissect the ceRNA network, we employed Cytoscape_(v3.6.1, Paul Shannon, Seattle, WA, USA), illustrating a comprehensive map for analysis.

2.6. Real-time quantitative reverse transcription-polymerase chainreaction (RT-qPCR)

For RT-qPCR validation, β-actin served as an internal control. Initially, 1 μg of RNA was reverse-transcribed into cDNA following the instructions provided by the TransScript reverse transcription kit (TransGen Biotech, AT311, Beijing, China). The primer sequences utilized in the RT-qPCR reaction, which had a total volume of 20 μL, are detailed in Table 1. The composition of the reaction mixture included 10 μL of PerfectStart Green qPCR SuperMix (IQ5TM, Bio-Rad, Hercules, CA, USA), 0.4 μL of 10 μM specific forward primer, 0.4 μL of 10 μM specific reverse primer, 2 μL of the reverse transcription product, and 7.2 μL of nuclease-free water. The thermal cycling conditions were set as follows: an initial pre-denaturation step at 94 °C for 30 s, followed by 40 cycles of denaturation at 94 °C for 5 s and annealing/extension at 60 °C for 30 s. The specificity of the amplified PCR product was verified by analyzing the melting curve. RT-qPCR analyses were performed on the LightCycler® 480 real-time PCR system (Roche Diagnostics, Indianapolis, IN, USA).) from Roche. Each sample was allocated three replicate wells, and the final Ct value for each sample was calculated by averaging the results from these replicates. The relative expression level of circRNA was quantified using the $2^{-\Delta\Delta Ct}$ method.

Table 1
Primers for RT-PCR

RNA name	Primers type	Primers sequence
hsa_circ_0069,399	Forward	AGACATCGACCTGTACCAGAGA
	Reverse	TTCTTCACAGTGACTGCTTTACC
circRNA43	Forward	AGCATCCTTGACTCCCCTTCTG
	Reverse	GGAGGGAAAATGAAGTCCAACG
hsa_circ_0001725	Forward	GGCAGTCACGTTTTTCGATGAT
	Reverse	TGGAAAGGTTTGAATACGGCTG
hsa_circ_0001789	Forward	GTCCCAGTGGGATGAAGATGAC
	Reverse	AACCTCAATTTCTCCTCGCTCC
hsa_circ_0000344	Forward	AGGTCAACAAGAACAAGGAAAT
	Reverse	CTGGGATGATCATCAGAGGAGG
hsa-miR-2110_R-1	Forward	TTGGGGAAACGGCCGC
	Reverse	GTGCAGGGTCCGAGGT

2.7. Statistical analysis

Data for each experimental set were derived from three biological replicates, ensuring robustness. Analysis was conducted utilizing both GraphPad Prism (V9.1.2, GraphPad Software, San Diego, California, USA) and SPSS statistical software (V11.0, IBM, Chicago, IL, USA). Results are presented as the mean ± standard deviation (x ± s). To evaluate the variation in expression of the target circRNA, we measured the fold change between the control and tumor groups. The significance of these differences was assessed using the two independent samples *t*-test, adopting a p-value <0.05 as the criterion for statistical significance.

3. Results

3.1. circRNA differential expression profile and visual analysis

To identify circRNAs specifically expressed in LSCC, we conducted high-throughput RNA sequencing on tissue samples from 10 LSCC patients (C1–C10) along with adjacent normal tissue samples (N1–N10). This approach facilitated a detailed analysis of circRNA expression profiles through microarray profiling. circRNAs that demonstrated a relative expression ratio exceeding one and displayed statistically significant differences ($P < 0.05$) were classified as differentially expressed. Utilizing parameters such as fold change (FoldChange) and p-value for the screening, we identified 126 circRNAs that met the criteria of having an absolute log2FoldChange

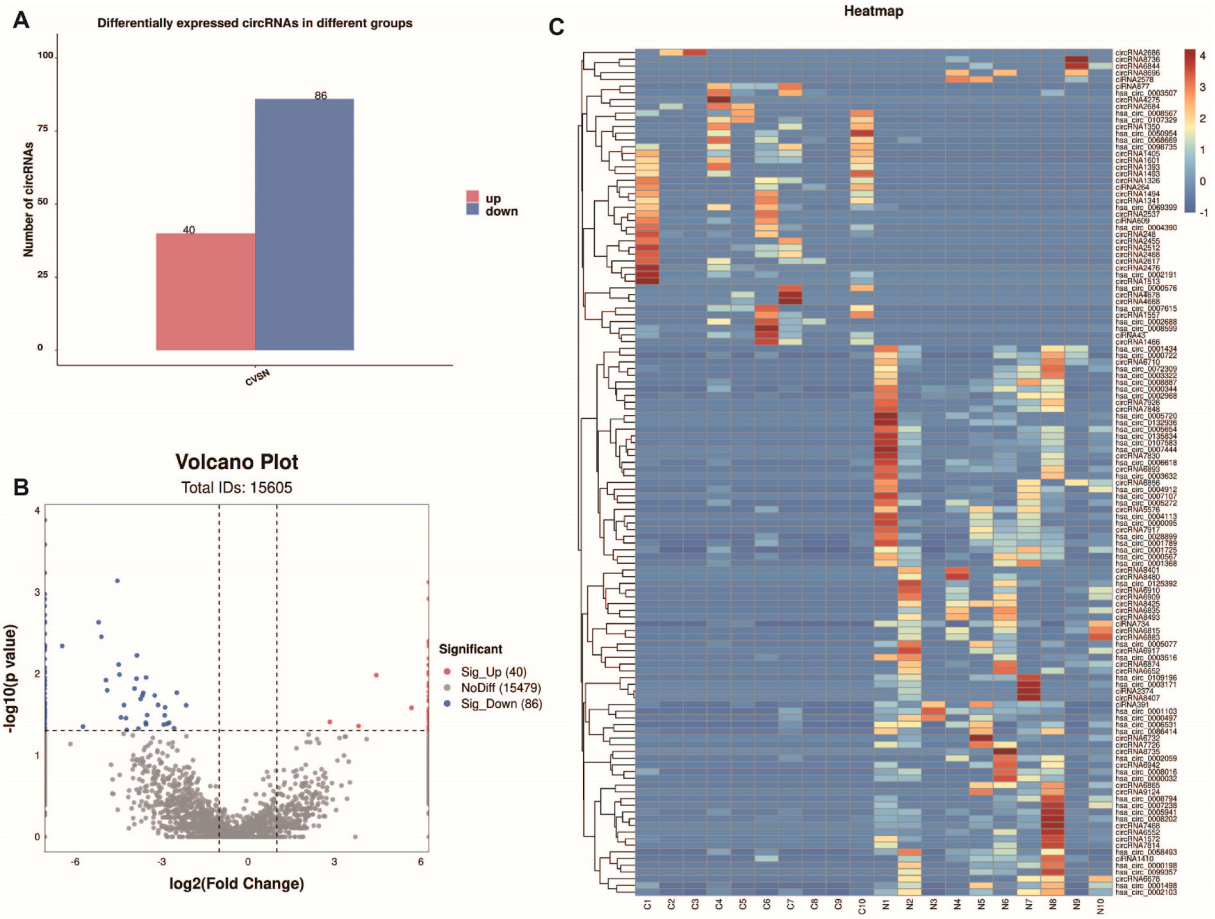

Fig. 1. circRNA differential expression profile and visual analysis. A, the differentially expressed circRNAs between LSCC tissues and adjacent normal tissues. The red columns indicate the number of up-regulated genes, while the blue columns indicate the number of down-regulated genes. B, Differentially expressed circRNA volcano maps. The volcano graph displays the fold change of differential gene expression in the comparison group on the x-axis, and the statistical significance of the difference in gene expression on the y-axis. In this graph, red indicates significantly up-regulated differentially expressed genes, blue represents significantly down-regulated differentially expressed genes, and gray represents non-significant differentially expressed genes. C, circRNA clustered analysis of differential expression. In the cluster diagram, the x-axis represents the sample, while the y-axis represents the screened differentially expressed genes. The different colors in the diagram represent different gene expression levels. The color scale ranges from blue to white to red, indicating the expression levels from low to high. Red color indicates high expressed genes, while blue color indicates low expressed genes.

value of at least 1 and a p-value less than 0.05. Among these, 40 circRNAs were found to be up-regulated, and 86 were down-regulated, (Fig. 1A) (Supplement Table S1).

To visualize the overall distribution of differentially expressed circRNAs, we constructed a volcano plot using log2 (fold change) as the x-axis and -log10 (*p*-value) as the y-axis (Fig. 1B). Differential gene cluster analysis was conducted to examine the clustering patterns of gene regulation under various experimental conditions. By clustering and analyzing genes based on the similarity of their expression profiles in different samples, we can visually represent the gene expression in different samples or treatment groups, thereby obtaining biologically relevant information. To better illustrate the clustering expression pattern, we displayed the gene expression of differential gene expression srpbm using Z values. The mapping data was screened based on significance, sorted by *p*-

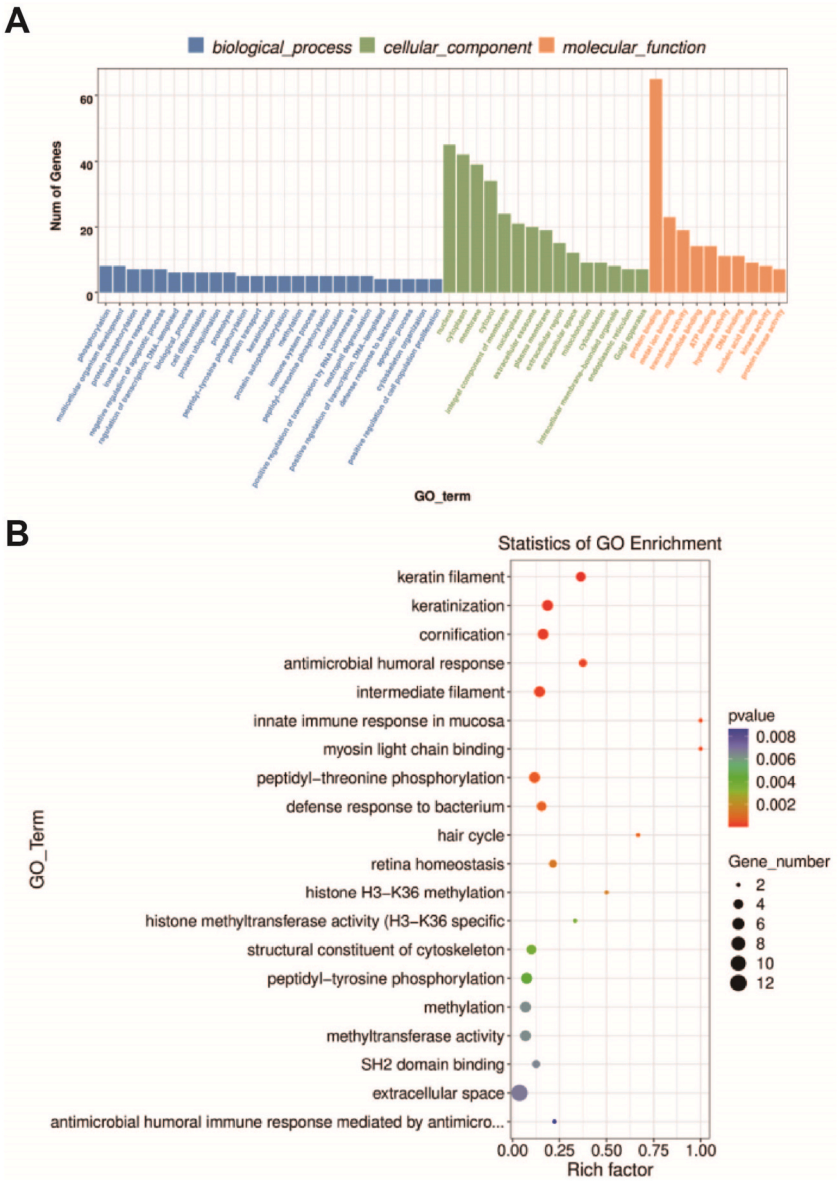

Fig. 2. GO enrichment analysis. A, GO Enrichment Analysis Histogram: The histogram visually segregates the genes into three main categories: molecular function, cellular component, and biological process, indicated along the x-axis. The y-axis illustrates how many differential genes are enriched within each specific Gene Ontology (GO) term, offering a clear distribution view. B, GO Enrichment Analysis Scatter Plot: This scatter plot demarcates the enrichment landscape of GO terms, with the x-axis displaying the Rich factor. The Rich factor quantifies the enrichment level, being the ratio of differential genes assigned to a GO term against the total gene count within that term — higher values suggest more substantial enrichment. On the y-axis, we have the GO_Term, denoting the functional annotation associated with each GO category. The diameter of each dot corresponds to the quantity of significantly differentiated genes aligned to an individual GO term, providing a visual measure of gene involvement. Dot coloration varies according to the p-value obtained from the enrichment analysis; colors representing a p-value below 0.05 signal statistically significant enrichment, enriching our understanding of the biological significance behind these genomic variations.

value from small to large, and a heat map was drawn (Fig. 1C).

3.2. GO enrichment analysis

We conducted a hypergeometric test to pinpoint GO terms significantly enriched among genes with substantial differential

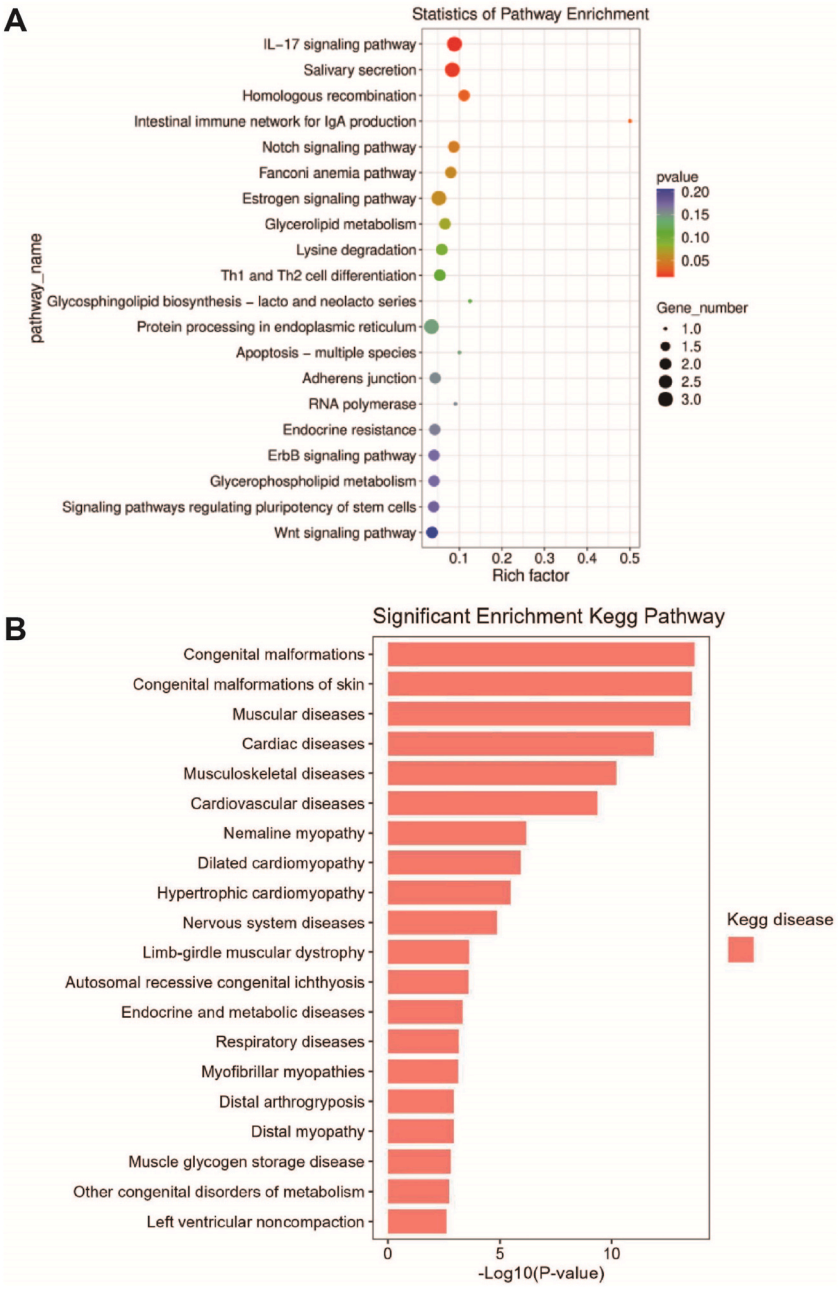

Fig. 3. KEGG enrichment analysis. A, Visualization of KEGG Pathway Enrichment Analysis. This scatter plot illustrates the correlation between the Rich factor and the specific KEGG pathway terms, where the Rich factor embodies the enrichment level in KEGG pathways — a higher Rich factor denotes more significant enrichment. The term "Pathway" specifically pertains to the various metabolic pathways cataloged by KEGG. Each point's size on the plot corresponds to the count of significantly differentiated genes aligned with any single KEGG category. Additionally, the color coding of each point signifies the p-value from the enrichment analysis; notably, points marked with a color representing a p-value lower than 0.05 are considered to exhibit significant enrichment. B, Analysis of Disease Enrichment in KEGG Terms. The bar chart from the KEGG disease enrichment analysis highlights the top 20 disease terms that show significant enrichment. This graphical representation not only identifies which diseases are most prominently associated with the enriched genes but also provides insights into potential pathological connections revealed through the study.

expression against the backdrop of the entire genome. These GO terms were organized in descending order according to the count of differentially expressed genes annotated under each term. The top 25, 15, and 10 GO terms were selected for graphical representation (Fig. 2A). Utilizing the ggplot2 package, results from the GO enrichment analysis were visually represented in a scatter plot. This plot

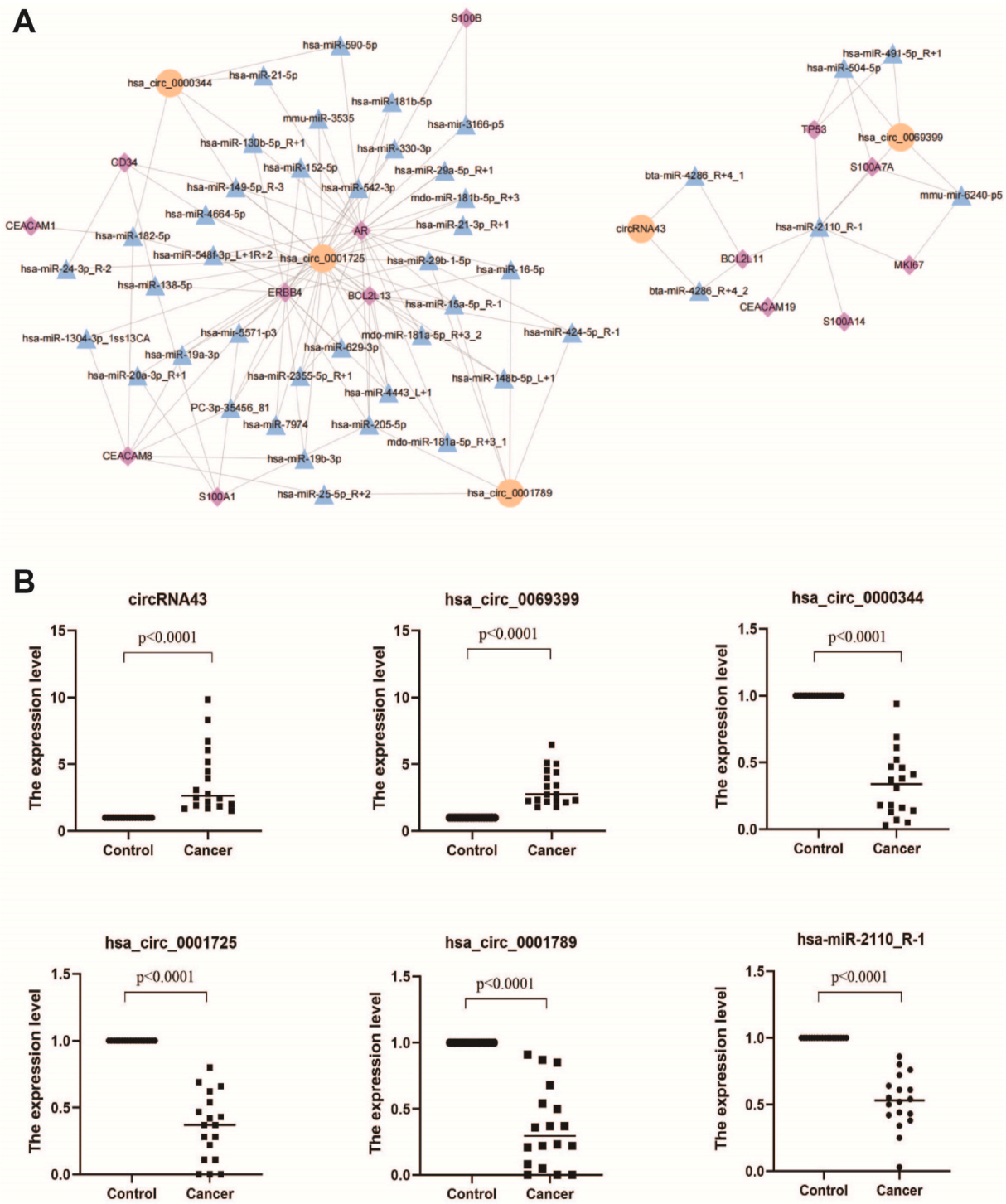

Fig. 4. CircRNA-mediated ceRNA network construction. A, Prediction of circRNA-miRNA-mRNA association: a. Down - regulated ceRNA network; b. Up - regulated ceRNA network; orange circles are circRNAs, blue triangles are miRNAs, and purple diamonds are mRNAs. B, Verification of target genes. The expression level of the target gene was verified by RT-qpcr. circRNA43 and hsa_circ_0069,399 are up-regulated, hsa_circ_0000344, hsa_circ_0001725, hsa_circ_0001789 and hsa-miR-2110_R-1 are down-regulated in LSCC tissue.

showcased the top 20 GO terms, ranked by the significance (p-value) of their enrichment (Fig. 2B).

3.3. KEGG enrichment analysis

Leveraging the ggplot2 software, we showcased the Kyoto Encyclopedia of Genes and Genomes (KEGG) pathway enrichment analysis findings through scatter plots. This visual representation highlighted the top 20 pathways, selected based on the significance (p-value) of their enrichment (Fig. 3A). For annotating differentially expressed circRNAs with KEGG disease-related pathways, we employed the KOABS3.0 online tool, referencing the gene set available on the KEGG Disease database. The analysis revealed enrichment in 290 disease pathways, encompassing a wide array of conditions such as head and neck cancers, digestive, respiratory, and urinary system cancers, among others. The most significant 20 pathways, prioritized by their enrichment p-values (Fig. 3B).

3.4. CircRNA-mediated ceRNA network construction

Utilizing five selected circRNAs and their corresponding target genes, we constructed a circRNA-miRNA-mRNA competitive endogenous RNA (ceRNA) regulatory network. This network comprised 62 nodes, including 5 circRNAs, 43 miRNAs, and 14 mRNAs (Fig. 4A). Notably, our analysis uncovered a competitive interaction within the ceRNA regulatory axis involving the genes KI67 and P53, and the circRNA hsa_circ_0069,399, both targeting the same miRNA, namely, hsa-miR-2110_R-1.

To validate the initial bioinformatics findings, we conducted RT-qPCR assays on these five circRNAs in 18 LSCC samples and their matched para-cancerous tissues. The validation revealed that, within the LSCC tissues, hsa_circ_0069,399 and circRNA43 were

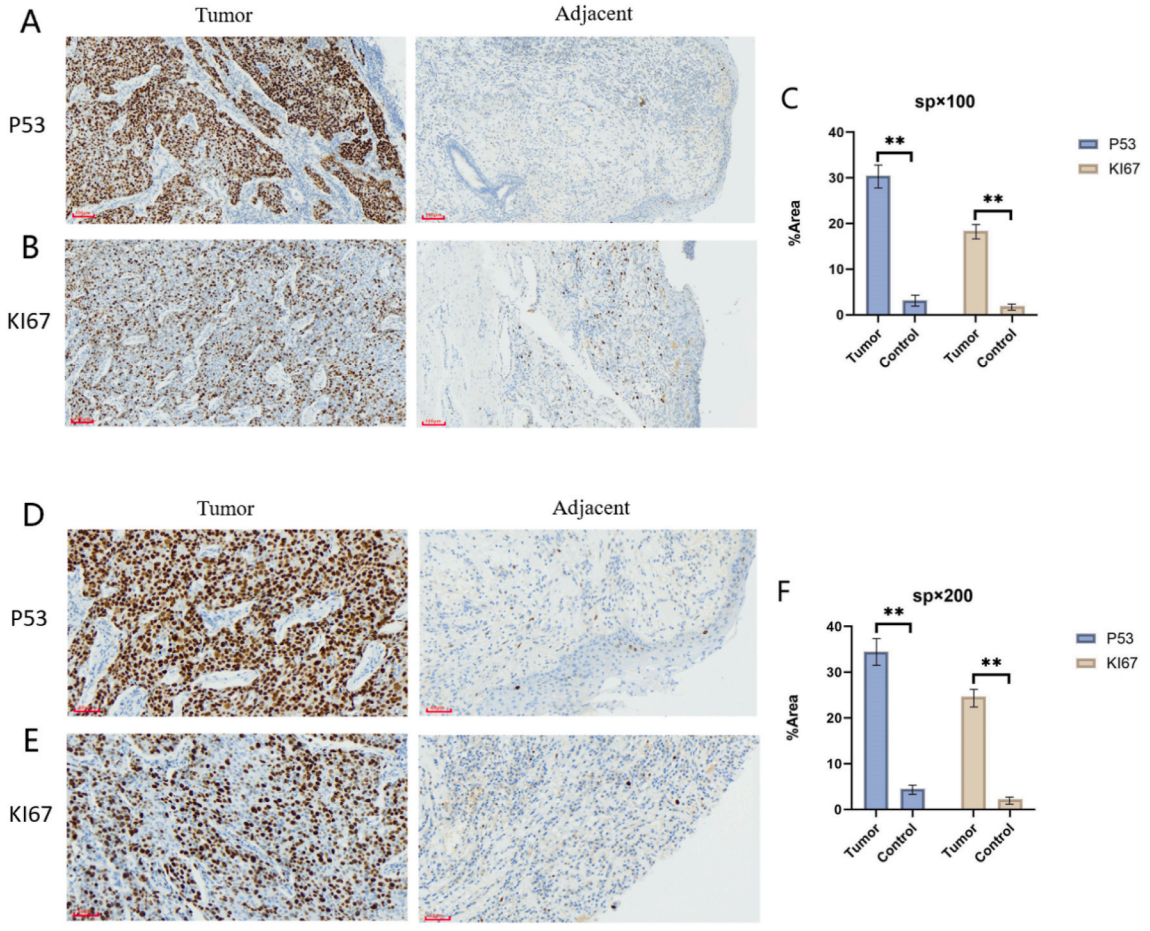

Fig. 5. Immunohistochemical Staining of KI67 and P53. (A) Demonstrates elevated expression of P53 in tumor tissues compared to adjacent non-tumor tissues, observed through immunohistochemistry at 10× magnification. (B) Illustrates higher levels of KI67 expression in tumor tissues relative to adjacent tissues, captured via immunohistochemistry at 10× magnification. (D) Reveals increased expression of P53 in tumor tissues over adjacent non-tumor tissues, visualized through immunohistochemistry at 20× magnification. (E) Shows augmented expression of KI67 in tumor tissues in comparison to neighboring tissues, as seen through immunohistochemistry at 20× magnification. (C)&(F) Display the quantified expression levels of P53 and KI67 in tumor tissues, confirmed by immunohistochemical analysis, with **P < 0.01 indicating a significant difference from adjacent non-tumor tissues. N = 10.

upregulated, whereas hsa_circ_0000344, hsa_circ_0001725, and hsa_circ_0001789 exhibited downregulation. Additionally, RT-qPCR verification was performed for hsa-miR-2110_R-1, which is targeted by hsa_circ_0069,399, in the same sets of tissue samples. The outcomes indicated a downregulation of hsa-miR-2110_R-1 expression in LSCC tissues, aligning with the patterns observed in our microarray analysis (Fig. 4B).

3.5. KI67 and P53 IHC staining

In the exploration of the molecular mechanisms underlying LSCC, the analysis of pivotal cell cycle regulators and tumor suppressor genes is essential. To this end, we specifically focused on KI67 and P53, two biomarkers renowned for their roles in cell proliferation and genomic stability, respectively. The inclusion of these markers in our study provides a direct link to understanding the proliferative capacity and potential dysregulation of cell cycle checkpoints in laryngeal cancer.

To investigate the expression levels of KI67 and P53, we employed immunohistochemical methods on cancerous and adjacent non-cancerous tissues from 10 patients diagnosed with LSCC. The staining outcomes, as illustrated in the corresponding figure, reveal a dark brown coloration indicative of KI67 and P53 expression in laryngeal cancer tissues. Conversely, the adjacent para-carcinoma tissues displayed a blue color, signifying the absence of these markers. This stark contrast highlights a significantly higher expression of KI67 and P53 in laryngeal cancer tissues compared to their non-cancerous counterparts, with statistical significance (P value $<$ 0.05, as shown in Fig. 5). Such findings underscore the potential of KI67 and P53 as biomarkers in the pathology of laryngeal cancer, further substantiating their role in the malignancy's cellular dynamics.

4. Discussion

Recent advancements have unveiled a novel family of endogenous non-coding RNAs known as circRNAs, which are formed via back splicing into closed covalent circular molecules. Predominantly localized in the cytoplasm and capable of being stored in exosomes, circRNAs primarily regulate gene expression by acting as molecular 'sponges' for miRNAs. This competition modulates the availability of miRNAs to their target mRNAs, thereby indirectly influencing mRNA expression [6,7]. The explosion of high-throughput sequencing and bioinformatics has facilitated the identification of numerous circRNAs, some of which are implicated in the progression or suppression of malignant tumors through various pathways [8].

Research into LSCC has particularly highlighted the intricate roles circRNAs play in cancer biology, affecting processes such as cell cycle arrest, proliferation, apoptosis, invasion, metastasis, and immune response [9,10]. Notably, certain circRNAs have been specifically associated with LSCC progression. For instance, overexpression of circZNF609 and CDR1as has been linked to tumor growth through specific miRNA interactions [11,12], while the downregulation of hsa_circ_0036,722 and silencing of hsa_circ_0005033 counteract tumor proliferation and enhance chemosensitivity, respectively [13,14]. Presently, the exploration of circRNAs in the context of LSCC is in its nascent stages. A myriad of circRNAs remains unidentified, with their potential roles and mechanisms in LSCC largely untapped. This scenario unfolds a broad spectrum of research opportunities, heralding a promising frontier in the study of circRNAs. Our study delves into the ceRNA hypothesis by exploring the competitive dynamics within the circRNA-miRNA-mRNA network in LSCC. Employing high-throughput sequencing, we have mapped out the differential expression profiles of circRNAs and, through subsequent bioinformatics analysis, identified key circRNAs that engage in a competitive relationship with pivotal cancer-related genes like KI67 and P53. Particularly, hsa_circ_0069,399 emerges as a central figure in this regulatory web, showcasing significant upregulation in LSCC tissues. This not only validates the ceRNA model but also aligns with our clinical observations, suggesting a mechanistic link to LSCC progression.

The distinguished roles of P53 and KI67 in cancer biology are well-documented, with their overexpression being a harbinger of aggressive disease and poor prognosis across various cancers [15–18]. In the context of LSCC, the heightened expression of these proteins, alongside the deregulation of hsa_circ_0069,399 and hsa-miR-2110_R-1, reinforces the potential of circRNAs as biomarkers for disease diagnosis and progression. This relationship underscores the clinical value of our findings and prompts further exploration into the role of circRNAs in cancer biology.

The research is constrained by its modest sample size, which may not fully represent the genetic diversity and complexity of laryngeal cancer across different populations. Additionally, the study's focus on circRNAs as potential tumor suppressors assumes a simplified view of cancer biology, which is known to be influenced by a myriad of factors including but not limited to genetic, epigenetic, and environmental contributors. Addressing these limitations in future research would be imperative to solidify the understanding of circRNAs' roles in LSCC and their potential as therapeutic targets or diagnostic markers.

5. Conclusion

In conclusion, our study sheds light on the intricate regulatory network of circRNA-miRNA-mRNA in LSCC, paving the way for novel diagnostic and therapeutic strategies. While our findings offer exciting prospects, the precise mechanisms through which circRNAs like hsa_circ_0069,399 drive LSCC development warrant deeper investigation. As research in this field progresses, circRNAs hold the promise of enriching our arsenal against LSCC, offering new avenues for improving patient outcomes.

Ethical approval

This study was approved by the Ethics Committee of the Yinchuan First People's Hospital (2022-147).

Funding

This research was supported by Ningxia Hui Autonomous Region Key R&D Program, China (2019BFG02001) and (2022BEG03103).

Disclosure statement

The authors declare no conflict of interest in this work.

Data availability statement

Data supporting the findings of this study are available from the corresponding author. The data associated with the study, although not deposited into a publicly available repository, are included in the article, supplementary material, and referenced in the article.

CRediT authorship contribution statement

Zhipeng Mi: Writing – review & editing, Writing – original draft, Investigation, Formal analysis, Data curation. **Wulin Wen:** Methodology, Investigation, Formal analysis, Data curation. **Fan Guo:** Software, Resources, Project administration, Methodology, Investigation. **Qiangyou Shi:** Writing – original draft, Visualization, Validation. **Chao Long:** Writing – original draft, Formal analysis, Data curation. **Yu Zhou:** Software, Resources, Methodology, Investigation. **Ruixia Ma:** Writing – review & editing, Writing – original draft, Funding acquisition, Conceptualization.

Declaration of competing interest

The authors declare that they have no known competing financial interests or personal relationships that could have appeared to influence the work reported in this paper.

References

[1] H.W. Schutte, F. Heutink, D.J. Wellenstein, et al., Impact of time to diagnosis and treatment in head and neck cancer: a systematic review, Otolaryngol. Head Neck Surg. 162 (4) (2020) 446–457.
[2] X.L. Pan, Y. Lin, The correct selection of treatment strategies for laryngeal cancer to improve the survival rate and quality of life for patients, Zhonghua er bi yan hou tou jing wai ke za zhi 55 (12) (2020) 1111–1115.
[3] L. Miao, G. Feng, H. Yuan, CircRNAs: a family number of miRNA regulatory transcriptome in laryngeal carcinoma, J. Clin. Lab. Anal. 35 (11) (2021) e24038.
[4] Z.X.G. Zheng, Treatment strategy and progress of laryngeal cancer, Modern oncology 30 (11) (2022) 2090–2093.
[5] A.R. Sharma, M. Bhattacharya, S. Bhakta, et al., Recent research progress on circular RNAs: biogenesis, properties, functions, and therapeutic potential, Mol. Ther. Nucleic Acids 25 (2021) 2162–2531 (Print)):355-371.
[6] C.X. Liu, L.L. Chen, Circular RNAs: characterization, cellular roles, and applications, Cell 185 (12) (2022) 2016–2034.
[7] H. Xu, M.D. Fang, C. Li, et al., Progress in research on the novel tumor marker circRNA, Zhongguo Yi Xue Ke Xue Yuan Xue Bao 43 (3) (2021) 435–444.
[8] L.S. Kristensen, T. Jakobsen, H. Hager, et al., The emerging roles of circRNAs in cancer and oncology, Nat. Rev. Clin. Oncol. 19 (3) (2021) 188–206.
[9] L. Chen, G. Shan, CircRNA in cancer: fundamental mechanism and clinical potential, Cancer Lett. 505 (2021) 49–57.
[10] S. Wu, X. Huang, X. Tie, et al., Role and mechanism of action of circular RNA and laryngeal cancer, Pathol. Res. Pract. 223 (2021) 153460.
[11] X. Yin, J. Wang, C. Shan, et al., Circular RNA ZNF609 promotes laryngeal squamous cell carcinoma progression by upregulating epidermal growth factor receptor via sponging microRNA-134-5p, Bioengineered 13 (3) (2022) 6929–6941.
[12] J. Zhang, H. Hu, Y. Zhao, et al., CDR1as is overexpressed in laryngeal squamous cell carcinoma to promote the tumour's progression via miR-7 signals, Cell Prolif. 51 (6) (2018) e12521.
[13] Y. Guo, Q. Huang, J. Zheng, et al., Diagnostic role of dysregulated circular RNA hsa_circ_0036722 in laryngeal squamous cell carcinoma, OncoTargets Ther. 13 (2020) 5709–5719.
[14] L. Gong, J. Chen, X. Jiang, Circ_0005033 is an oncogene in laryngeal squamous cell carcinoma and regulates cell progression and Cisplatin sensitivity via miR-107/IGF1R axis, Anti Cancer Drugs 33 (3) (2022) 245–256.
[15] B.P. Lalkota, B.J. Srinivasa, M.V. Swamy, et al., The role of p53 and ki67 in predicting clinical outcome in breast cancer patients, J. Cancer Res. Therapeut. 19 (2) (2023) 208–213.
[16] D. Rusu-Andriesi, A.M. Trofin, M. Zabara, et al., Does the overall survival of the resectable periampullary carcinomas correlate with high expression of p53 and ki67? Chirurgia 117 (4) (2022) 423–430.
[17] O. Helminen, J. Melkko, J. Saarnio, et al., Predictive value of p53, Ki67 and TLR5 in neoplastic progression of Barrett's esophagus: a matched case-control study, Virchows Arch. 481 (3) (2022) 467–476.
[18] X. Zhang, Z. Wu, Y. Peng, et al., Correlationship between Ki67, VEGF, and p53 and hepatocellular carcinoma recurrence in liver transplant patients, BioMed Res. Int. 2021 (2021) 6651397.